

Designing Superionic Conductors Using Tetrahedrally Packed Structures

Tomoyasu Yokoyama^{1*}, Kazuhide Ichikawa¹, Takuya Naruse¹,
Kosei Ohura¹, Yukihiro Kaneko¹

^{1*}Technology Division, Panasonic Holdings Corporation, 1006 Kadoma,
Kadoma City, Osaka 571-8508, Japan.

*Corresponding author(s). E-mail(s):
yokoyama.tomoyasu@jp.panasonic.com;

Abstract

In the pursuit of advanced energy storage solutions, the crystal structure of ionic conductors plays a pivotal role in facilitating ion transport. The conventional structural design principle that compounds with the body-centered cubic (BCC) anionic frameworks have high ionic conductivity is well known. We have extended the conventional design principle by uncovering that many of the anionic frameworks of Ag-ion conductors are characterized by tetrahedrally packed (TP) structures. Leveraging our findings, we have virtually screened TP framework compounds, uncovering their intrinsic potential for superior ionic conductivity through first-principles molecular dynamics simulations. Our design principle is applicable to Ag^+ and other mobile ions, including Li^+ and F^- . We proposed the Met2Ion method to generate ionic crystal structures using metal crystal structures as templates and demonstrated that new ionic conductors with TP frameworks can be discovered. This work paves the way for the discovery and development of next-generation energy storage materials with enhanced performance.

Keywords: Solid-state electrolyte, Ionic conductivity, Framework topology, Tetrahedrally packed structure, First-principle calculation, Crystal structure generation

1 Introduction

The incessant drive for innovation in energy storage technologies has positioned ionic conductivity as a cornerstone material property, especially for applications in fuel cells

and batteries [1, 2]. In this regard, the structural design of ion conductors has emerged as a critical area of research, with the aim of enhancing the performance and safety of these devices. The significance of the crystal structure in influencing ionic transport is well-recognized, and a substantial body of work has been devoted to the exploration of Li-ion conductors, given their central role in all-solid-state Li-ion batteries [3–7].

Previous research has established that the topology of the framework composed of non-mobile ions in ionic conductors affects its ability to mobile ions [8]. Specifically, studies have highlighted that body-centered cubic (BCC) frameworks, composed solely of tetrahedral sites, enable more efficient ion transport than other structures like face-centered cubic (FCC) or hexagonal close-packed (HCP) frameworks. As shown in Figure 1a, the tetrahedron in the HCP structure shares a face with one tetrahedron and three octahedra. The mobile ions at the tetrahedral site must pass through an octahedral site to diffuse outward. Different site energies, including those of the tetrahedral and octahedral sites, lead to greater energy gaps to the transition state for ion diffusion, which leads to lower ionic conductivity. In contrast, the BCC structure is composed of tetrahedra only, and mobile ions can diffuse from one tetrahedral site to another tetrahedral site without passing through octahedral sites, as shown in Figure 1b. Therefore, because the site energy remains constant, the energy barrier for ionic diffusion is lower in the BCC anionic framework than that in the HCP framework. In fact, the experimental values for AgI ionic conductivity within the HCP and BCC anionic frameworks are 10^{-4} S/cm and 1 S/cm, respectively, at about 420 K [9], showing significantly higher Ag-ion conductivity with a BCC framework. This principle has also been applied to Li-ion conductors like $\text{Li}_{10}\text{GeP}_2\text{S}_{12}$, which possess BCC frameworks and offer high Li-ion conductivity, promising safer solid electrolyte candidates for all-solid-state Li-ion batteries [4, 6]. These insights are crucial for designing materials with high ionic conductivity for advanced energy storage applications.

The following questions then arise: What is the ideal structure for high ionic conductivity, and could it be a BCC framework structure? To explore this, our research turns to the Ag-ion conductors, known for their exceptional ionic conductivities, with the aim of identifying framework structures that could serve as templates for new superionic materials. While research in the literature so far has extensively examined the topology of Li-ion conductors, Ag-ion conductors have received less attention. Yet, compounds like RbAg_4I_5 exhibit remarkably high Ag-ion conductivity [10], about ten times greater than their Li-ion conductors [4, 6]. By delving into the structural intricacies of Ag-ion conductors, we aim to broaden the understanding of ionic conductivity and potentially discover universal design principles applicable to various ionic conductors.

Our study introduces a new structural design principle highlighting the significance of tetrahedrally packed (TP) frameworks for high ionic conductivity. Our analysis revealed that many of the anionic frameworks of high Ag-ion conductors are characterized by TP structures. The TP structure, which is composed entirely of tetrahedral tiling, is regarded as a superordinate concept to the BCC structure. For example, the RbAg_4I_5 structure shown in Figure 1c features an anionic framework of the β -Mn-type structure, which belongs to the TP structure family. While it was previously known in a limited context that argyrodite-type ionic conductors exhibit high conductivity

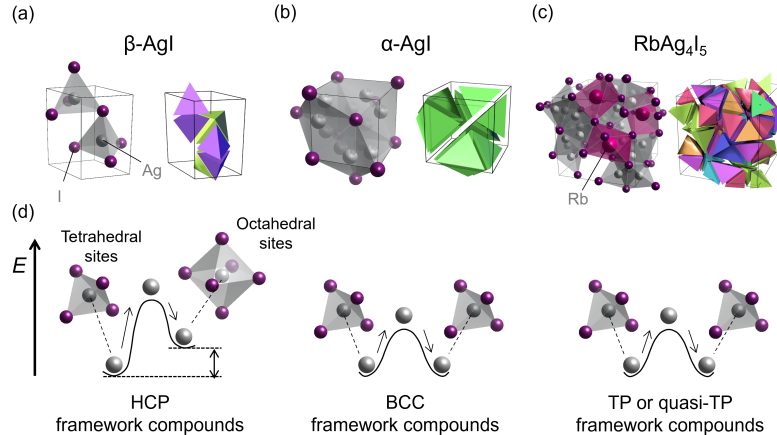


Fig. 1 Crystal structures and polyhedral tiling of (a) β -AgI with a hexagonal close-packed (HCP) framework, (b) α -AgI with a body-centered cubic (BCC) framework, and (c) RbAg_4I_5 with a quasi-tetrahedrally packed (TP) framework. (d) Conceptual diagram illustrating the migration barriers for Ag-ion diffusion within these frameworks.

due to their tetrahedrally close-packed (TCP) framework—a specialized subgroup of TP structures—there hasn’t been much discussion about other TP frameworks [11–13]. Armed with the insight that TP framework structures could be key to achieving high ionic conductivity, we embarked on a systematic screening of TP framework compounds from experimental databases. Our first-principles molecular dynamics (FPMD) calculations confirmed that these compounds exhibit high ionic conductivity across various mobile ion species, not just limited to Ag^+ ions. This finding is significant as it suggests that the TP framework is a universal design motif for high conductivity, applicable to both anion and cation conductors.

To further the discovery of unknown superionic conductors with this new design principle, we introduced the Met2Ion method, a novel crystal structure design approach inspired by the structural parallels between metallic and ionic crystals. Our Met2Ion method transcends the capabilities of conventional template-based prediction methods, enabling the prediction of previously unknown ionic crystal structures. Employing the Met2Ion method, we successfully identified novel Li-ion compounds with TP frameworks that exhibit high ionic conductivity, demonstrating our method’s efficacy in virtual screening. The implications of this work are profound, as it not only enhances the understanding of ionic conductivity but also provides a powerful tool for the discovery of novel superionic conductors. Our study thus sets a new precedent for the efficient development of ionic conductors, paving the way for the next generation of energy storage technologies.

2 Results

2.1 Identification of framework structures of Ag-ion conductors

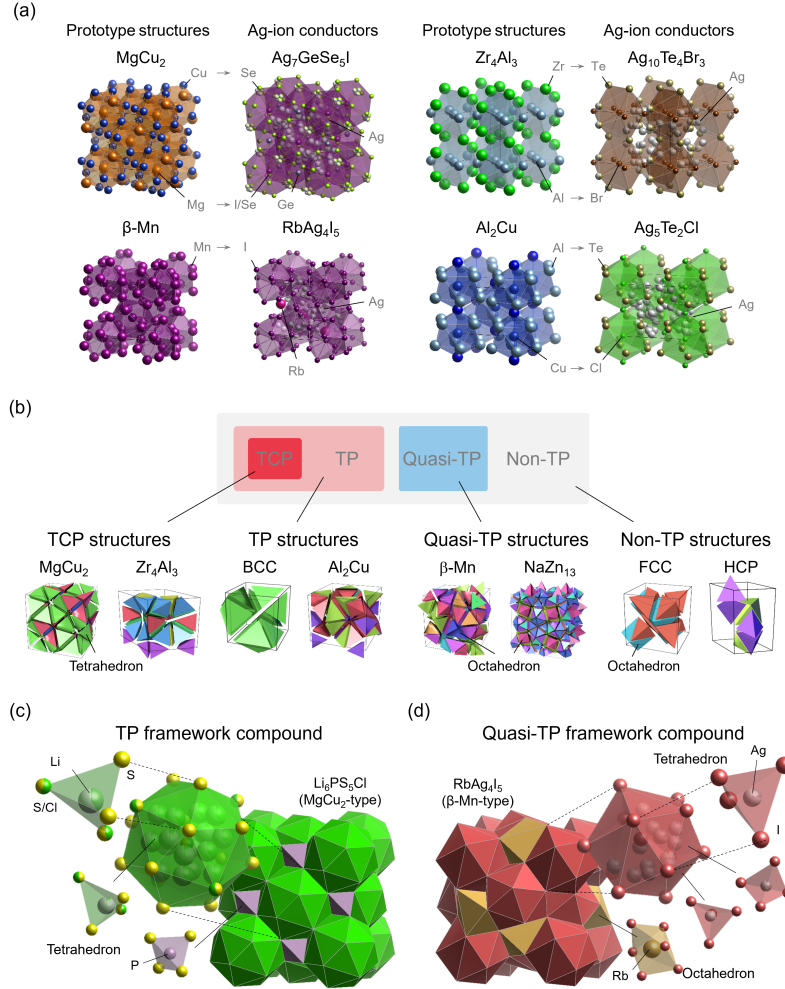


Fig. 2 (a) Prototype structures and their corresponding Ag-ion conductors, including $\text{Ag}_7\text{GeSe}_5\text{I}$ with a MgCu_2 -type framework, $\text{Ag}_{10}\text{Te}_4\text{Br}_3$ with a Zr_4Al_3 -type framework, RbAg_4I_5 with a $\beta\text{-Mn}$ -type framework, and $\text{Ag}_5\text{Te}_2\text{Cl}$ with an Al_2Cu -type framework. (b) Classification of structures based on space-filling polyhedra and example of polyhedral tiling of tetrahedrally close-packed (TCP), tetrahedrally packed (TP), quasi-TP, and non-TP structures. (c) A crystal structure composed of $\text{Li}_6\text{PS}_5\text{Cl}$ with a MgCu_2 -type framework. (d) A crystal structure of RbAg_4I_5 with a $\beta\text{-Mn}$ -type framework.

Our research began by examining the structure of Ag-ion conductors, which are known for their outstanding ionic conductivity. We sourced the crystal structures of these conductors from the Inorganic Crystal Structure Database (ICSD) [14] and analyzed them to identify their anionic framework prototypes. Through this analysis, we found that many of these conductors have BCC anionic frameworks, known to yield high ionic conductivity. For instance, AgI and Ag₃SI both have BCC anionic frameworks and demonstrate high Ag-ion conductivities of 1 S/cm at 420 K [9] and 3.8×10^{-2} S/cm [15], respectively. These insights, compiled in Table S1, reconfirm the promising role of BCC anionic frameworks in crafting materials with superior conductivity, aligning with established design principles.

In addition, our research identified superionic conductors that are different from the BCC framework. For instance, Ag₇GeSe₅I exhibits an Ag-ion conductivity of 4.3×10^{-2} S/cm [16] and has an anionic framework of MgCu₂-type structure called cubic Laves phase. Ag₁₀Te₄Br₃ shows an Ag-ion conductivity of 1.4×10^{-2} S/cm at room temperature [17] and has a Zr₄Al₃-type framework. RbAg₄I₅, with a conductivity of 2.1×10^{-1} S/cm at room temperature [10] and has a β -Mn-type framework. Additionally, Ag₅Te₂Cl has an Ag-ion conductivity of 1.0×10^{-1} S/cm at 341 K [18] and has a Al₂Cu-type framework. These diverse structures, illustrated in Figure 2a, all represent significant departures from the BCC framework, demonstrating the variety of crystal structures leading to high ionic conductivity.

To comprehend the characteristics of these prototype structures that diverge from the BCC framework, we encountered insights from Bonneau *et al.*'s study on metallic crystals [19]. Their study indicated that structures such as MgCu₂, Zr₄Al₃, and Al₂Cu are classified as tetrahedrally packed (TP) structures, which can be filled with slightly distorted tetrahedra [22]. The BCC structure is a unique TP structure composed of all congruent tetrahedra. Meanwhile, other structures, such as the MgCu₂-type, are also categorized within the TP family but are specifically known as Frank-Kasper structures or tetrahedrally close-packed (TCP) structures—a concept first introduced by Frank and Kasper in the 1950s. Specifically, a structure is recognized as a TCP structure if it features a pattern where five or six tetrahedra meet at an edge [22, 23]. These TCP structures have unique coordination polyhedra, referred to as Frank-Kasper polyhedra. Their report by Bonneau *et al.* expands on TP structures, including quasi-TP structures that are predominantly tetrahedral but may contain other polyhedra, such as in β -Mn and NaZn₁₃.

Figures 2b display various structural types, including TCP, TP, quasi-TP, and non-TP structures. TP structures like BCC and MgCu₂-type are filled with tetrahedra, unlike FCC and HCP structures. The Li₆PS₅Cl structure has a MgCu₂-type anionic framework with multiple tetrahedra [12], as seen in Figure 2c. Here, Li atoms are located at two tetrahedral sites within a Frank-Kasper polyhedron. The tetrahedra around Li atoms form a three-dimensional network without interference from the P atom tetrahedra. The RbAg₄I₅ anionic framework, depicted in Figure 2d, is a quasi-TP structure with six types of tetrahedra and an octahedron, making up 96% tetrahedral sites. The tetrahedra around Ag atoms form a three-dimensional network without interference from the Rb atom octahedra. Table 1 presents a selection of other TP prototype structures and related ionic crystals.

Table 1 List of reported tetrahedrally packed (TP), tetrahedrally close-packed (TCP), and quasi-TP structures. In the “Category” column, “TP”, “TCP”, and “q-TP” refer to the TP, TCP, and quasi-TP structure, respectively. N_{atom} means the number of atoms in the unit cell. “Relevant ionic crystal” refers to a representative ionic crystal that has the same anionic or cationic framework as the structure of its metallic crystal. Elements that compose the framework in the compound are shown in bold.

Category	Structure type	Space group	N_{atom}	Relevant ionic crystal	Ref.
TP	BCC	$Im\bar{3}m$	2	Ag I , Ca TiO ₃	[19]
TCP	MgCu ₂	$Fd\bar{3}m$	24	Ag ₇ Ge Se ₅ I , Mg Al ₂ O ₄	[19, 20]
TCP	MgZn ₂	$P6_3/mmc$	12	Li ₆ Si O ₄ Cl ₂ , Na Be ₄ Sb O ₇	[19, 20]
TCP	MgNi ₂	$P6_3/mmc$	24	Mg ₃ Be Al ₈ O ₁₆	[20]
TCP	Cr ₃ Si	$Pm\bar{3}m$	8	Cu ₆ Te ₃ S , Y ₃ Al ₅ O ₁₂	[19, 20]
TCP	Zr ₄ Al ₃	$P6/mmm$	7	Ag ₁₀ Te ₄ Br ₃ , Ba Ti ₂ Fe ₄ O ₁₁	[19, 20]
TCP	Mg ₄ Zn ₇	$C2/m$	110	-	[20]
TCP	Co ₈ Mn ₉ Si ₃	$Pnmm$	74	-	[20]
TCP	Na ₅₂ Au ₈₁ Si ₂₉	$Im\bar{3}$	162	-	[20]
TCP	Ti ₂ (Ni,Al,Ti) ₃	$C2/m$	50	-	[20]
TCP	K ₇ Cs ₆	$P6_3/mmc$	26	SrFe ₁₂ O ₁₉	[20]
TCP	Th ₆ Cd ₇	$Pbam$	26	-	[20]
TCP	W ₆ Fe ₇	$R\bar{3}m$	39	Ag ₁₉ Te ₆ Br ₇ , K ₂ Al _{11-x} O ₁₇	[20]
TCP	Nb ₄₈ Ni ₃₉ Al ₁₃	$Pnma$	52	Ag ₁₉ Br _{5.438} I _{1.562} Te ₆	[20]
TCP	Mg ₂₃ Al ₃₀	$R\bar{3}$	159	-	[20]
TCP	Mn ₇₇ Fe ₄ Si ₁₉	$C2$	110	-	[20]
TCP	Cr ₉ Mo ₂₁ Ni ₂₀	$Pnma$	56	-	[20]
TCP	MoNi	$P2_12_12_1$	56	-	[20]
TCP	Mn ₈₂ Si ₁₈	$Immm$	186	-	[20]
TCP	β -U	$P4_2/mnm$	30	NF ₃	[20]
TP	Al ₂ Cu	$I4/mcm$	12	Ag ₅ Te ₂ Cl , Pb ₃ O ₄	[19]
TP	CaCu ₅	$P6/mmm$	6	Cd ₃ P Cl ₃	[19]
TP	AlB ₂	$P6/mmm$	3	PbSb ₂ O ₆	[19]
TP	ThSi ₂	$I4_1/amd$	12	Na ₃ N ₈	[19]
TP	FeB	$Pnma$	8	Li ₂ IOH , BaSO ₄	[19]
TP	CrB	$Cmcm$	8	Li(NH ₃) I , KClO ₃	[19]
TP	CeNi ₃	$P6_3/mmc$	24	-	[19]
TP	PuNi ₃	$R\bar{3}m$	36	CuTi ₂ S ₄	[19]
TP	Ce ₂ Ni ₇	$P6_3/mmc$	36	-	[19]
TP	Th ₂ Ni ₁₇	$P6_3/mmc$	38	-	[19]
TP	Th ₂ Zn ₁₇	$R\bar{3}m$	57	-	[19]
q-TP	β -Mn	$P4_132$	20	RbAg ₄ I ₅ , Ag ₄ TeSO ₄	[21]
q-TP	BaCd ₁₁	$I4_1/amd$	48	-	[19]
q-TP	NaZn ₁₃	$Fm\bar{3}c$	112	Mg ₃ B ₇ O ₁₃ Cl , Ag ₁₃ OsO ₆	[19]
q-TP	ThMn ₁₂	$I4/mmm$	26	-	[19]

While the individual anionic frameworks of Li₆PS₅Cl and RbAg₄I₅, as well as their high ionic conductivity, were known [12, 24], our discovery lies in conceptualizing these and other frameworks as the broader TP structure family. Our findings highlight TP structures as a key to designing high-performance ionic conductors, extending beyond the BCC structures, due to their potential for lower ion migration barriers. Therefore, in response to the question presented in the introduction regarding what constitutes an ideal structure for high ionic conductors, TP framework structures have emerged as a promising answer.

2.2 Screening of TP framework compounds with mobile cations and anions

To verify the hypothesis that TP frameworks lead to high ionic conductivity, we analyzed TP compounds from the ICSD using FPMD calculations. First, we focused on cases where the anion forms the framework and the cation is mobile. We extracted compounds with an anionic framework matching the TP structures from the ICSD and evaluated their ionic conductivities through FPMD simulations. Figure 3a displays a histogram of these compounds, categorized by mobile ion species. The most commonly identified anionic framework was the MgCu_2 -type structure, with the argyrodite-type ionic structure being a representative example of an ionic compound with this anionic framework. Argyrodite-type ionic compounds have been recognized for their superionic conductivity in Cu and Ag compounds since the 1970s [25] and similar high Li-ion conductivity was reported in 2008 [3], sparking extensive research and a surge in these compounds.

We evaluated the ionic conductivities of TP framework compounds through FPMD calculations. Table 2 summarizes compounds with conductivities over 1.0×10^{-4} S/cm, alongside experimental values. Complete data is available in Table S2. Figures 3c-f show the crystal structures of typical TP anionic framework compounds and the mobile ion probability densities from FPMD simulations. Arrhenius plots from these simulations are in Figure S1.

Argyrodite-type compounds with MgCu_2 -type frameworks, such as $\text{Ag}_7\text{GeSe}_5\text{I}$ and $\text{Li}_6\text{PS}_5\text{Cl}$, exhibit high theoretical and experimental ionic conductivities. $\text{Li}_7\text{N}_2\text{I}$, another MgCu_2 -type framework compound, which is not argyrodite-type, demonstrates high theoretical conductivity. Additionally, compounds with TCP structures, including MgZn_2 , Cr_3Si , Zr_4Al_3 , and W_6Fe_7 frameworks, show potential for high ionic conductivity. For instance, $\text{Ag}_{19}\text{Te}_6\text{Br}_7$ features a W_6Fe_7 -type framework with Te and Br substituting for W and Fe. $\text{Li}_3(\text{NH}_2)_2\text{I}$ features a MgZn_2 -type framework with I and NH_2 atoms substituting for Mg and Zn, respectively. Similarly, $\text{Li}_6\text{SiO}_4\text{Cl}$ possesses a MgZn_2 -type framework where Cl and O ions replace Mg and Zn atoms. Compounds with frameworks composed of TP structures, such as $\text{Ag}_5\text{Te}_2\text{Cl}$ with an Al_2Cu -type framework, also displayed high ionic conductivities. $\text{Li}_6\text{B}_7\text{S}_{13}\text{I}$, derived from NaZn_{13} with S and I substitutions, showed a theoretical Li-ion conductivity of 2.1×10^{-3} S/cm. Cd-ion compounds typically exhibit low ionic conductivity due to the large ionic radius and strong Coulomb interactions of Cd^{2+} ions. However, $\text{Cd}_{13}\text{P}_4\text{S}_{22}\text{I}_2$ with a TP framework is theoretically predicted to have high ionic conductivity. This suggests that TP frameworks can enhance ionic conductivity in compounds with various cations.

We also studied cases where the cation forms the framework and the anion is mobile. Figure 3b displays a histogram categorizing these compounds, highlighting a greater prevalence of cationic frameworks compared to anionic frameworks. Since these compounds with TP cationic framework are typical ionic crystal structures such as spinel-type, pyrochlore-type, and garnet-type, the number of candidate structures is larger than in the case of the anionic framework. Among the compounds extracted in this case, NaSn_2F_5 and KSbF_4 , which have been reported as F-ion conductors, are shown in Figure 3g and 3h as an example. KSbF_4 has a distorted FeB-type framework in which the Fe and B atoms in FeB are replaced with K and Sb atoms, respectively.

Table 2 Summary of the calculated and experimental ionic conductivities and activation energies of the tetrahedrally packed (TP) framework compounds. “Ion” refers to a possible mobile ion in the compound. “Formula” refers to the compositional formula of the calculated structure. “ICSD ID” refers to the database collection code. “Framework type” refers to the structural type of the anionic framework for each compound. σ_{300K} and $E_{a,300K}$ mean the ionic conductivity at room temperature and the activation energy as extrapolated from Arrhenius plots based on first-principle molecular dynamics (FPMD) calculations, respectively. σ_{exp} is the reported ionic conductivity. When the temperature is not stated, the ionic conductivity is at room temperature.

Ion	ICSD ID	Formula	Framework type	σ_{300K} (S/cm)	$E_{a,300K}$ (eV)	σ_{exp} (S/cm)	Ref.
Ag ⁺	241154 ^a	Ag ₇ GeSe ₅ I	MgCu ₂	4.6×10^{-2}	0.158	4.3×10^{-2}	[16]
Ag ⁺	418781	Ag ₁₀ Te ₄ Br ₃	Zr ₄ Al ₃	3.8×10^{-2}	0.169	1.4×10^{-2}	[17]
Ag ⁺	421400	Ag ₅ Te ₂ Cl	Al ₂ Cu	1.5×10^{-2}	0.206	1.0×10^{-1} @341K	[18]
Ag ⁺	419160	Ag ₁₉ Te ₆ Br ₇	W ₆ Fe ₇	7.2×10^{-2}	0.158	1.1×10^{-2} @323K	[26]
Ag ⁺	27203	RbAg ₄ I ₅	β -Mn	4.8×10^{-2}	0.139	2.1×10^{-1}	[10]
Cu ⁺	418657 ^a	Cu ₆ PS ₅ Cl	MgCu ₂	9.6×10^{-4}	0.275	4.7×10^{-4}	[11]
Cu ⁺	88660	Cu ₈ CeSe ₆	MgZn ₂	4.6×10^{-4}	0.403	-	-
Cu ⁺	427561	Cu ₆ Te ₃ S	Cr ₃ Si	8.5×10^{-3}	0.246	-	-
Cu ⁺	610355	Cu ₆ SbAs	Cr ₃ Si	7.7×10^{-4}	0.233	-	-
Cu ⁺	140304	Cu ₉ Te ₄ Cl ₃	Zr ₄ Al ₃	4.1×10^{-2}	0.177	-	-
Cu ⁺	51911	KCu ₄ I ₅	β -Mn	3.2×10^{-2}	0.164	6.1×10^{-1} @540K	[24]
Li ⁺	418490 ^a	Li ₆ PS ₅ Cl	MgCu ₂	1.1×10^{-2}	0.180	5.0×10^{-3}	[27]
Li ⁺	85713	Li ₇ N ₂ I	MgCu ₂	1.1×10^{-3}	0.281	-	-
Li ⁺	167528	Li ₃ (NH ₂) ₂ I	MgZn ₂	5.3×10^{-3}	0.217	1.7×10^{-5}	[28]
Li ⁺	143283	Li ₆ SiO ₄ Cl ₂	MgZn ₂	3.5×10^{-4}	0.199	6.2×10^{-6} @575K	[29]
Li ⁺	143928	Li ₆ B ₇ S ₁₃ I	NaZn ₁₃	2.1×10^{-3}	0.247	5.0×10^{-4}	[30]
Cd ²⁺	622	Cd ₁₃ P ₄ S ₂₂ I ₂	MgCu ₂	6.6×10^{-4}	0.279	-	-
F ⁻	14136	NaSh ₂ F ₅	Al ₂ Cu	1.8×10^{-3}	0.432	4.1×10^{-7} @373K	[31]
F ⁻	431489	KSbF ₄	FeB	1.5×10^{-3}	0.332	1.0×10^{-4}	[32]

^a Since numerous argyrodite-type ionic compounds were identified, Table 2 includes only one result per mobile ion species.

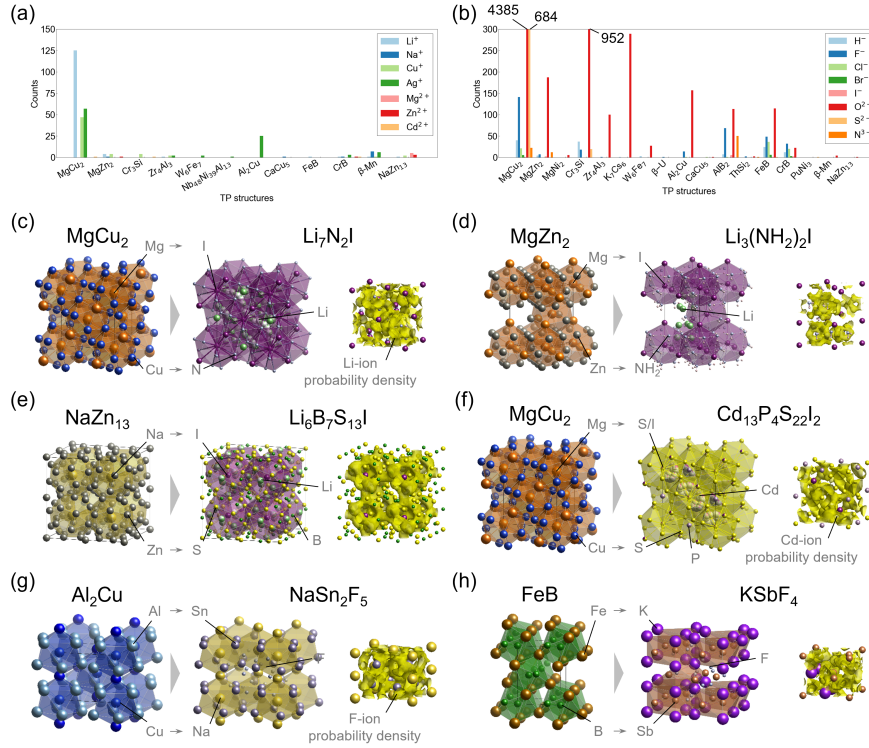


Fig. 3 Histograms of (a) tetrahedrally packed (TP) anionic framework compounds and (b) TP cationic framework compounds in the ICSD. Structures of the TP metallic compounds and TP framework compounds and ionic conductive pathways of TP framework compounds in (c) $\text{Li}_7\text{N}_2\text{I}$ with MgCu_2 -type framework, (d) $\text{Li}_3(\text{NH}_2)_2\text{I}$ with MgZn_2 -type framework, (e) $\text{Li}_6\text{B}_7\text{S}_{13}\text{I}$ with NaZn_{13} -type framework, (f) $\text{Cd}_{13}\text{P}_4\text{S}_{22}\text{I}_2$ with MgCu_2 -type framework, (g) NaSn_2F_5 with Al_2Cu -type framework, and (h) KSbF_4 with FeB -type framework.

NaSn_2F_5 has a Al_2Cu -type framework in which the Al and Cu atoms in Al_2Cu are replaced with Sn and Na atoms, respectively. The F-ion conductivities of these compounds at room temperature obtained from the FPMD calculations were over 10^{-3} S/cm. Due to the large number of candidate structures and the high computational cost, comprehensive screening of anionic conductors with TP framework structures is reserved for our future work.

Additionally, it should be noted that compositional design could enhance the ionic conductivity of TP framework compounds. For instance, despite having a MgCu_2 -type anionic framework, $\text{Li}_3\text{N}_2\text{Te}$ exhibited negligible Li-ion conduction in our calculations, which can be attributed to a high number of mobile ions occupying tetrahedral sites, leaving few vacancies for ion diffusion. FPMD calculations indicate that decreasing the number of Li-ions can lead to enhanced conductivity, as demonstrated in Figure

S2. These findings indicate that TP framework compounds, previously considered low ionic conductors, may possess high conductivity potential with the right compositional design.

We comment here on the effectiveness of FPMD calculations in predicting ionic conductivity. Although there are some differences between experimental and theoretical ionic conductivities, our computational results align with the overall trends observed in experimental data, as also advocated in the literature [33]. It is true that potential deviations can stem from impurities, grain boundaries, and synthesis-related variations [34]; however, FPMD calculations remain a useful predictive tool for ionic conductivities.

Thus, our investigation reveals that TP framework compounds demonstrate high theoretical ionic conductivity, irrespective of the mobile ion being an anion or cation. These insights offer a novel design principle for ionic conductors, potentially superseding traditional BCC framework guidelines.

2.3 Search for unknown TP framework compounds via rule-based structure generation

To bridge the gap in discovering unsynthesized TP framework compounds with high ionic conductivity, we developed the Met2Ion method for designing such materials. In the preceding section, we identified high ionic conductors from a pool of experimentally synthesized compounds with known TP structures. However, this method cannot uncover TP framework compounds that remain unsynthesized. The recent synthesis of $\text{Li}_6\text{SiO}_4\text{Cl}_2$ with a MgZn_2 -type framework and $\text{Li}_6\text{B}_7\text{S}_{13}\text{I}$ with a NaZn_{13} -type framework suggests a wealth of undiscovered TP framework compounds with potentially high ionic conductivity [29, 30]. To address this gap, we introduce a new rule-based scheme, the Met2Ion method, for generating the crystal structures of such unknown TP framework compounds, inspired by the structural relationship between metallic and ionic crystals.

Our Met2Ion method employs a systematic process of elemental substitution and atomic arrangement, using metallic crystal structures as blueprints to create ionic crystal structures. We applied this approach to discover novel, synthesizable Li-ion compounds within the TP framework that exhibit high ionic conductivity. The steps of the Met2Ion method, detailed in Figure 4a, include:

1. Replacing metal elements with anions in TP structures (e.g., MgZn_2 to $\text{O}_4\text{Cl}_2^{10-}$).
2. Inserting non-mobile cations into tetrahedral sites of the anionic framework (e.g., $\text{O}_4\text{Cl}_2^{10-}$ to $\text{SiO}_4\text{Cl}_2^{6-}$).
3. Adding mobile ions to tetrahedral sites to maintain electrical neutrality (e.g., $\text{SiO}_4\text{Cl}_2^{6-}$ to $\text{Li}_6\text{SiO}_4\text{Cl}_2$).
4. Conducting structural optimization through first-principles calculations to assess thermodynamic stability.
5. Evaluating ionic conductivity using FPMD calculations.

The rationale behind structure generation from Steps 1 to 3 is founded on the resemblance between TP metallic and TP ionic crystals. For instance, $\text{Li}_6\text{SiO}_4\text{Cl}_2$ is derived from an MgZn_2 -type framework by substituting metal atoms with Cl and O

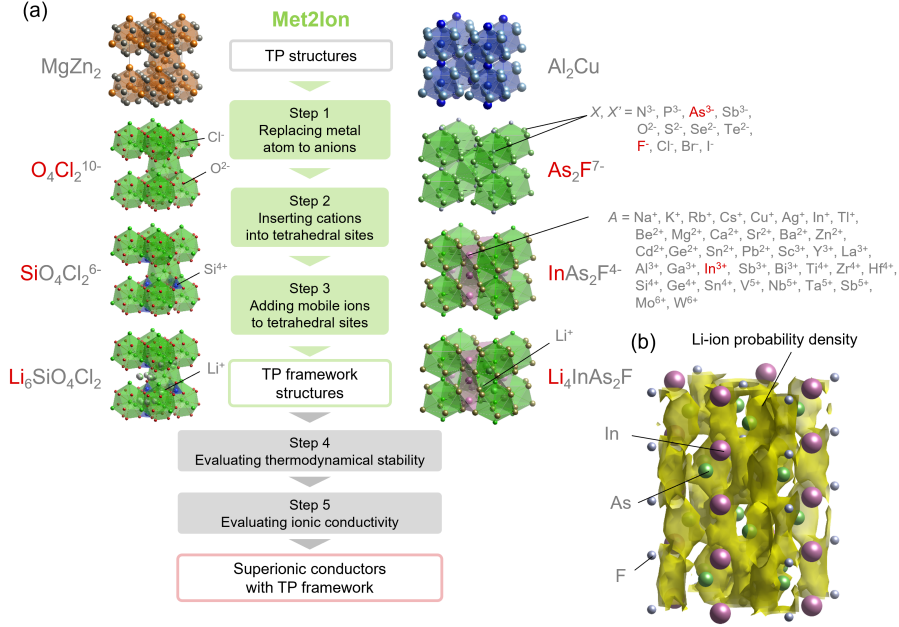


Fig. 4 (a) Search flow for tetrahedrally packed (TP) framework compounds using the Met2Ion method, which involves the following procedure to obtain Li₆SiO₄Cl₂ from MgZn₂ and the hypothetical Li₄InAs₂F from Al₂Cu: Step 1 is to replace the metal atoms of the TP structures with two anions, X and X', with candidate anions for X and X' shown. In Step 2, a non-mobile cation A is placed at the tetrahedral site, with the candidate cations for A as shown. In Step 3, mobile cations are placed at the remaining tetrahedral sites to achieve electroneutrality. In Step 4, thermodynamically stable compounds are screened by performing ab initio calculations. In Step 5, compounds with high ionic conductivity are screened using first-principles molecular dynamics (FPMD) calculations. (b) Li-ion conductivity path of one of the compounds obtained, Li₄InAs₂F.

and introducing Li and Si at tetrahedral sites to achieve charge balance. This process is guided by the principle of substituting ions while preserving the elemental ratio seen in the metallic parent structure. Subsequently, we assess the thermodynamic stability and ionic conductivity of each candidate structure using first-principles calculations.

Considering Figure 3a, which shows the Al₂Cu-type as a the second most common, our search extended to various Li_xAX₂X' compounds, with A as a cation and X, X' as anions. Table S3 and Figure S3 list the compounds identified through this screening. Six Al₂Cu-type framework compounds emerged as viable candidates for synthesis, with theoretical ionic conductivities surpassing 1.0×10⁻³ S/cm at room temperature and convex hull energies below 0.1 eV/atom. Notably, Li₄InAs₂F exhibited a convex hull energy under 0.1 eV/atom and an impressive ionic conductivity of 8.0×10⁻² S/cm. The crystal structure of Li₄InAs₂F, depicted in Figure 4a, is characterized by an Al₂Cu-type framework forming a dodecahedron of As and F atoms. The primary

Li-ion diffusion pathways in $\text{Li}_4\text{InAs}_2\text{F}$ run along the c-axis, as shown in Figure 4b, facilitated by the face-sharing connectivity of tetrahedral sites.

While we have focused on the Al_2Cu -type structure, our scheme is adaptable to other frameworks and mobile ions, holding promise for unveiling more high ionic conductors. We recently established a method to generate crystal structures from polyhedra via discrete geometry analysis [35] which enables to generate new TP prototype structures. The Met2Ion method surpasses traditional template-based prediction methods by enabling the discovery of ionic crystal structures that are not readily inferred from simple elemental substitutions [36]. This study not only furnishes a blueprint for designing ionic conductive materials but also introduces an innovative method for predicting the structures of as-yet unknown TP framework compounds.

3 Discussion

We have proposed a new design principle based on the fact that TP framework compounds exhibit high ionic conductivity, and through crystal structure design based on this principle, we have designed ionic conductors that could not be found via conventional compositional design methods. First, we focused on the framework topology of Ag-ion conductors, which have been reported to have the highest available ionic conductivity. We found that many Ag-ion conductors have a TP framework, along with a BCC framework, which was also known to allow high ionic conductivity. Second, we showed that this design principle can be applied not only to Ag^+ ions, but also to other ions, including Li^+ and F^- . Therefore, TP framework compounds can serve as a universal structural design principle for the development of superionic conductors. Third, we have proposed a method for virtual screening of TP structures and TP framework compounds to aid in the discovery of new TP framework compounds. We have demonstrated that it is possible to discover new Li-ion conductors theoretically that are synthesizable and that show high ionic conductivity using our Met2Ion method. The results of this work offer the potential to create novel solid electrolytes with superionic conductivity for any mobile ionic species and to aid in the development of energy storage devices, including batteries and fuel cells.

4 Methods

Data preparation and analysis

The raw data of the crystal structures were exported from the Inorganic Crystal Structure Database (ICSD), version 2023.1, using the API [14]. Among the structures that were labeled “structure type” in the database, structures composed of metal or metalloid elements and containing more than five data were extracted as “ICSD prototype structures”. The total number of prototype structures extracted was 621. Among the Ag-ion compounds in the ICSD, those with titles that included the words “superionic”, “solid electrolyte”, “ion conductor”, and “ion conductivity” in the titles of their original papers were extracted, and data other than solid electrolyte materials were removed. Compounds with a framework that matched the prototype structure were then extracted as Ag-ion conductors using the StructureMatcher function [37]

implemented in Pymatgen [38]. Based on the charge information for the atoms in the structure file, negatively charged ions (anions) were considered as the framework ions, and positively charged ions (cations) were removed. We use StructureMatcher with `ltol = 0.2`, `stol = 0.3`, and `angle_tol = 2`. If there are partially occupied sites in the structure, the sites were merged using the `merge_sites` function with `mod = average` and `tol = 1`. The total number of extracted Ag-ion conductors was 45. Ionic compounds with TP framework were extracted from ICSD under the same conditions. The visualizations were performed using VESTA, 3dt, and Systre software [39, 40].

Ionic conductivity and probability density calculations

Density functional theory (DFT) calculations were performed using the Vienna Ab initio Simulation Package (VASP) with the projector augmented-wave approach and Perdew-Burke-Ernzerhof (PBE) generalized gradient approximation (GGA) functions [41–44]. For the first-principles molecular dynamics (FPMD), a supercell model was created such that one side was larger than 8 Å. Non-spin-polarized DFT calculations were performed using a k-point at the center of Γ . The time step was set to 2 fs. When the partially occupied structure was calculated, the method of Bushlanov *et al.* [45] was used to obtain the most symmetrical atomic configuration, and this configuration was used as the initial structure. For the virtual structure, the lattice constants were fixed at those obtained after structural relaxation, but for the ICSD data, the lattice constants were fixed at the experimental values. The reason for the use of these constants is that the symmetry and the lattice constants after structural relaxation change depending on the initial atomic configuration when the partially occupied structure is calculated, which then affects the ion conductivity. Ion diffusion was evaluated using an NVT ensemble controlled by a Nosé-Hoover thermostat over a temperature range of 400 K to 900 K. The total time to convergence for the diffusivity ranged from 90 ps to 200 ps. Results at temperatures at which the framework structure melted (`max_framework_displacement` was greater than 5 Å) were removed. The first 5000 steps were removed to ensure thermal equilibrium, and the diffusion coefficients and ionic conductivities were calculated from the resulting mean-square displacement (MSD). The ion probability densities were obtained from FPMD calculations performed at the highest temperatures at which the framework did not collapse. The activation energies were obtained using the Nernst-Einstein equation. The ionic conductivity values were plotted versus the reciprocal of temperature to obtain the room-temperature ionic conductivity. The ionic probability density values within a structure were calculated by subdividing the supercell into a grid of cubic cells with an edge length of 0.2 Å, and counting the number of time steps for which an ion occupies each cell. We used the diffusion analyzer in Pymatgen [38] to perform these analyses.

Crystal structure generation and screening

The structure of an unknown TP framework compound was predicted using our proposed Met2Ion method, inspired by the structural rules for metallic and ionic crystals. Structure generation was performed in Steps 1, 2, and 3. In Step 1, the composition

of the TP metallic crystal was maintained and the metallic atoms were replaced with anions. The Al and Cu atoms in Al_2Cu were replaced with two different anions. The candidate anions were N^{3-} , P^{3-} , As^{3-} , Sb^{3-} , O^{2-} , S^{2-} , Se^{2-} , Te^{2-} , F^- , Cl^- , Br^- and I^- . In Step 2, the non-mobile cation was placed at the tetrahedral site with the lowest multiplicity of the Wyckoff label (site 4a in the Al_2Cu case). This is because the higher the number of non-mobile cations in the unit cell, the lower the ionic conductivity. The candidates for the non-mobile cations are: Na^+ , K^+ , Rb^+ , Cs^+ , Cu^+ , Ag^+ , In^+ , Tl^+ , Be^{2+} , Mg^{2+} , Ca^{2+} , Sr^{2+} , Ba^{2+} , Zn^{2+} , Cd^{2+} , Ge^{2+} , Sn^{2+} , Pb^{2+} , Sc^{3+} , Y^{3+} , La^{3+} , Al^{3+} , Ga^{3+} , In^{3+} , Sb^{3+} , Bi^{3+} , Ti^{4+} , Zr^{4+} , Hf^{4+} , Si^{4+} , Ge^{4+} , Sn^{4+} , V^{5+} , Nb^{5+} , Ta^{5+} , Sb^{5+} , Mo^{6+} , and W^{6+} . In Step 3, the movable ions were arranged to maintain electrical neutrality. Ideally, the most energetically stable atomic configuration should be identified from all combinations of atomic configurations. However, in view of the computational costs, the atomic configuration for the Li^+ ions in this work was determined from the most symmetrical structure using the method of Bushlanov *et al.* [45]. Screening of the generated structures is performed in Steps 4 and 5. In Step 4, the thermodynamic stability of the crystal structure generated in Step 3 was evaluated via first-principles calculations. From a potential pool of 38 cations and 12 anions, a total of 5472 candidate compositions were calculated. The generated structures were subjected to structural relaxation and single-point calculations while symmetry was maintained. Competing phases were extracted from compounds with a convex hull energy of 0 eV/atom in the Materials Project [46], and structural relaxation and one-point calculations were also performed. DFT calculations were performed under essentially the same conditions that were used in the Materials Project [46]. Structures with a convex hull energy of 0.1 eV/atom or less were selected as the synthesizable compounds [47]. The number of candidate compounds extracted in Step 4 was 84. In Step 5, ionic conductivity was evaluated for the structures obtained in Step 4 by performing FPMD calculations. There were 6 candidate compounds obtained in Step 5 that theoretically had an ionic conductivity greater than 1.0×10^{-3} S/cm at room temperature.

Supplementary information. List of Ag-ion conductors extracted from ICSD; list of the calculated ionic conductivities and activation energies of the Ag-, Cu-, Li-, Na-, Zn-, Cd-, Mg-, and F-ion TP framework compounds; List of Li-ion conductor candidates with Al_2Cu -type framework screened using the Me2Ion method; Crystal structures of MgCu_2 and $\text{Li}_8\text{N}_2\text{Te}$ with MgCu_2 -type framework; Li-ion diffusion paths and mean square displacement (MSD) of Li ions of $\text{Li}_8\text{N}_2\text{Te}$ and $\text{Li}_7\text{N}_2\text{Te}$; Arrhenius plots of $\text{Li}_7\text{N}_2\text{Te}$ obtained by FPMD calculations; and Arrhenius plots for virtual TP framework compounds obtained by FPMD calculations.

References

- [1] Knauth, P.: Inorganic solid li ion conductors: An overview. *Solid State Ionics* **180**(14-16), 911–916 (2009) <https://doi.org/10.1016/j.ssi.2009.03.022>
- [2] Minh, N.Q.: Ceramic Fuel Cells. *Journal of the American Ceramic Society* **76**(3), 563–588 (1993) <https://doi.org/10.1111/j.1151-2916.1993.tb03645.x>

- [3] Deiseroth, H.J., Kong, S.T., Eckert, H., Vannahme, J., Reiner, C., Zaiß, T., Schlosser, M.: $\text{Li}_6\text{PS}_5\text{X}$: A Class of Crystalline Li-Rich Solids With an Unusually High Li^+ Mobility. *Angewandte Chemie* **47**(4), 755–758 (2008) <https://doi.org/10.1002/anie.200703900>
- [4] Kato, Y., Hori, S., Saito, T., Suzuki, K., Hirayama, M., Mitsui, A., Yonemura, M., Iba, H., Kanno, R.: High-power all-solid-state batteries using sulfide superionic conductors. *Nature Energy* **1**(4), 1–7 (2016) <https://doi.org/10.1038/nenergy.2016.30>
- [5] Asano, T., Sakai, A., Ouchi, S., Sakaida, M., Miyazaki, A., Hasegawa Asano, S.T., Sakai, A., Ouchi, S., Sakaida, M., Miyazaki, A., Hasegawa, S.: Solid halide electrolytes with high lithium-ion conductivity for application in 4v class bulk-type all-solid-state batteries. *Advanced Materials* **30**, 1803075 (2018) <https://doi.org/10.1002/adma.201803075>
- [6] Li, Y., Song, S., Kim, H., Nomoto, K., Kim, H., Sun, X., Hori, S., Suzuki, K., Matsui, N., Hirayama, M., Mizoguchi, T., Saito, T., Kamiyama, T., Kanno, R.: A lithium superionic conductor for millimeter-thick battery electrode. *Science* **381**(6653), 50–53 (2023) <https://doi.org/10.1126/science.add7138>
- [7] Tanaka, Y., Ueno, K., Mizuno, K., Takeuchi, K., Asano, T., Sakai, A.: New Oxyhalide Solid Electrolytes with High Lithium Ionic Conductivity $>10 \text{ mS cm}^{-1}$ for All-Solid-State Batteries. *Angewandte Chemie* **135**(13), 1–5 (2023) <https://doi.org/10.1002/ange.202217581>
- [8] Wang, Y., Richards, W.D., Ong, S.P., Miara, L.J., Kim, J.C., Mo, Y., Ceder, G.: Design principles for solid-state lithium superionic conductors. *Nature Materials* **14**(10), 1026–1031 (2015) <https://doi.org/10.1038/nmat4369>
- [9] Tubandt, C., Lorenz, E.: The molecular condition and electrical conductivity of crystallized salts. *Zeitschrift für Physikalische Chemie* **87**, 513–542 (1914)
- [10] Owens, B.B., Argue, G.R.: High-Conductivity Solid Electrolytes: Mg_4I_5 . *Science* **157**(3786), 308–310 (1967) <https://doi.org/10.1126/science.157.3786.308>
- [11] Kuhs, W.F., Nitsche, R., Scheunemann, K.: The argyrodites - A new family of tetrahedrally close-packed structures. *Materials Research Bulletin* **14**(2), 241–248 (1979) [https://doi.org/10.1016/0025-5408\(79\)90125-9](https://doi.org/10.1016/0025-5408(79)90125-9)
- [12] Morgan, B.J.: Mechanistic Origin of Superionic Lithium Diffusion in Anion-Disordered $\text{Li}_6\text{PS}_5\text{X}$ Argyrodites. *Chemistry of Materials* **33**(6), 2004–2018 (2021) <https://doi.org/10.1021/acs.chemmater.0c03738>
- [13] Han, G., Vasylenko, A., Daniels, L.M., Collins, C.M., Corti, L., Chen, R., Niu, H., Manning, T.D., Antypov, D., Dyer, M.S., *et al.*: Superionic lithium transport via multiple coordination environments defined by two-anion packing. *Science*

383(6684), 739–745 (2024) <https://doi.org/10.1126/science.adh5115>

- [14] Bergerhoff, G., Hundt, R., Sievers, R., Brown, I.D.: The Inorganic Crystal Structure Data Base. *Journal of Chemical Information and Computer Sciences* **23**(2), 66–69 (1983) <https://doi.org/10.1021/ci00038a003>
- [15] Gombotz, M., Hanghofer, I., Eisbacher-Lubensky, S., Wilkening, H.: Ionic and electronic transport in the fast Ag^+ conductor α^* - Ag_3SI . *Solid State Sciences* **118**, 106680 (2021) <https://doi.org/10.1016/j.solidstatesciences.2021.106680>
- [16] Belin, R., Zerouale, A., Pradel, A., Ribes, M.: Ion dynamics in the argyrodite compound $\text{Ag}_7\text{GeSe}_5\text{I}$: Non-Arrhenius behavior and complete conductivity spectra. *Solid State Ionics* **143**(3-4), 445–455 (2001) [https://doi.org/10.1016/S0167-2738\(01\)00883-9](https://doi.org/10.1016/S0167-2738(01)00883-9)
- [17] Lange, S., Nilges, T.: $\text{Ag}_{10}\text{Te}_4\text{Br}_3$: A new silver(I) (poly)chalcogenide halide solid electrolyte. *Chemistry of Materials* **18**(10), 2538–2544 (2006) <https://doi.org/10.1021/cm060226m>
- [18] Nilges, T., Nilges, S., Pfitzner, A., Doert, T., Böttcher, P.: Structure-Property Relations and Diffusion Pathways of the Silver Ion Conductor $\text{Ag}_5\text{Te}_2\text{Cl}$. *Chemistry of Materials* **16**(5), 806–812 (2004) <https://doi.org/10.1021/cm031131c>
- [19] Bonneau, C., O’Keeffe, M.: Intermetallic crystal structures as foams. beyond frank-kasper. *Inorganic Chemistry* **54**(3), 808–814 (2015) <https://doi.org/10.1021/ic5017966>
- [20] Sikirić, M.D., Delgado-Friedrichs, O., Deza, M.: Space fullerenes: A computer search for new Frank-Kasper structures. *Acta Crystallographica Section A* **66**(5), 602–615 (2010) <https://doi.org/10.1107/S0108767310022932>
- [21] Karlsen, O.B., Kjekshus, A., Romming, C., Rost, E.: The crystal structure of the low temperature $\text{Au}_{80-v}\text{Cu}_v\text{Sn}_{20}$ Phase. *Acta Chemica Scandinavica* **46**, 1076–1082 (1992) <https://doi.org/10.3891/acta.chem.scand.46-1076>
- [22] O’Keeffe, M.: Sphere Packings and Space Filling by Congruent Simple Polyhedra. *Acta Crystallographica Section A* **54**(3), 320–329 (1998) <https://doi.org/10.1107/S0108767397017893>
- [23] Shoemaker, D.P., Shoemaker, C.B.: Concerning the relative numbers of atomic coordination types in tetrahedrally close packed metal structures. *Acta Crystallographica Section B* **42**(1), 3–11 (1986) <https://doi.org/10.1107/S0108768186098671>
- [24] Hull, S., Keen, D.A., Sivia, D.S., Berastegui, P.: Crystal Structures and Ionic Conductivities of Ternary Derivatives of the Silver and Copper Monohalides: I.

- Superionic Phases of Stoichiometry MA_4I_5 : $RbAg_4I_5$, KAg_4I_5 , and KCu_4I_5 . *Journal of Solid State Chemistry* **165**(2), 363–371 (2002) <https://doi.org/10.1006/JSSC.2002.9552>
- [25] Kuhs, W.F., Nitsche, R., Scheunemann, K.: The crystal structure of Cu_6PS_5Br , a new superionic conductor. *Acta Crystallographica Section B* **34**(1), 64–70 (1978) <https://doi.org/10.1107/S0567740878002307>
- [26] Nilges, T., Messel, J., Bawohl, M., Lange, S.: Silver(I) Chalcogenide Halides $Ag_{19}Te_6Br_7$, $Ag_{19}Te_6Br_{5.4}I_{1.6}$, and $Ag_{19}Te_5SeBr_7$. *Chemistry of Materials* **20**(I), 4080–4091 (2008) <https://doi.org/10.1021/cm800425u>
- [27] Yu, C., Ganapathy, S., Hageman, J., Van Eijck, L., Van Eck, E.R.H., Zhang, L., Schwietert, T., Basak, S., Kelder, E.M., Wagemaker, M.: Facile Synthesis toward the Optimal Structure-Conductivity Characteristics of the Argyrodite Li_6PS_5Cl Solid-State Electrolyte. *ACS Applied Materials and Interfaces* **10**(39), 33296–33306 (2018) <https://doi.org/10.1021/acsami.8b07476>
- [28] Matsuo, M., Sato, T., Miura, Y., Oguchi, H., Zhou, Y., Maekawa, H., Takamura, H., Orimo, S.I.: Synthesis and lithium fast-ion conductivity of a new complex hydride $Li_3(NH_2)_2I$ with double-layered structure. *Chemistry of Materials* **22**(9), 2702–2704 (2010) <https://doi.org/10.1021/cm1006857>
- [29] Morscher, A., Dyer, M.S., Duff, B.B., Han, G., Gamon, J., Daniels, L.M., Dang, Y., Surta, T.W., Robertson, C.M., Blanc, F., Claridge, J.B., Rosseinsky, M.J.: $Li_6SiO_4Cl_2$: A Hexagonal Argyrodite Based on Antiperovskite Layer Stacking. *Chemistry of Materials* **33**(6), 2206–2217 (2021) <https://doi.org/10.1021/acs.chemmater.1c00157>
- [30] Kaup, K., Bishop, K., Assoud, A., Liu, J., Nazar, L.F.: Fast Ion-Conducting Thioboracite with a Perovskite Topology and Argyrodite-like Lithium Substructure. *Journal of the American Chemical Society* **143**(18), 6952–6961 (2021) <https://doi.org/10.1021/jacs.1C00941>
- [31] Patro, L.N., Hariharan, K.: Frequency dependent conduction characteristics of mechanochemically synthesized $NaSn_2F_5$. *Materials Science and Engineering: B* **162**(3), 173–178 (2009) <https://doi.org/10.1016/J.MSEB.2009.04.003>
- [32] Kawahara, K., Ishikawa, R., Nakayama, K., Shibata, N., Ikuhara, Y.: Room temperature fluoride ion conductivity in defective β - $KSb_{1-\delta}F_{4-3\delta}$ polycrystals. *Journal of Power Sources* **483**(31), 229173 (2021) <https://doi.org/10.1016/j.jpowsour.2020.229173>
- [33] Zhu, Z., Deng, Z., Chu, I.-H., Radhakrishnan, B., Ping Ong, S.: Ab initio molecular dynamics studies of fast ion conductors. *Computational Materials System Design*, 147–168 (2018) https://doi.org/10.1007/978-3-319-68280-8_7

- [34] Nolan, A.M., Zhu, Y., He, X., Bai, Q., Mo, Y.: Computation-accelerated design of materials and interfaces for all-solid-state lithium-ion batteries. *Joule* **2**(10), 2016–2046 (2018) <https://doi.org/10.1016/j.joule.2018.08.017>
- [35] Yokoyama, T., Ichikawa, K., Naito, H.: Crystal structure generation based on polyhedra using dual periodic graphs. *Crystal Growth & Design* **24**(5), 2168–2178 (2024) <https://doi.org/10.1021/acs.cgd.3c01492>
- [36] Liu, C., Tamaki, H., Yokoyama, T., Wakasugi, K., Yotsuhashi, S., Kusaba, M., Yoshida, R.: Shotgun crystal structure prediction using machine-learned formation energies. *arXiv* (2023) <https://doi.org/10.48550/arXiv.2305.02158>
- [37] Hundt, R., Schön, J., Jansen, M.: Cmpz—an algorithm for the efficient comparison of periodic structures. *Journal of applied crystallography* **39**(1), 6–16 (2006) <https://doi.org/10.1107/S0021889805032450>
- [38] Ong, S.P., Richards, W.D., Jain, A., Hautier, G., Kocher, M., Cholia, S., Gunter, D., Chevrier, V.L., Persson, K.A., Ceder, G.: Python Materials Genomics (pymatgen): A robust, open-source python library for materials analysis. *Computational Materials Science* **68**, 314–319 (2013) <https://doi.org/10.1016/j.commatsci.2012.10.028>
- [39] Momma, K., Izumi, F.: VESTA: A three-dimensional visualization system for electronic and structural analysis. *Journal of Applied Crystallography* **41**(3), 653–658 (2008) <https://doi.org/10.1107/S0021889808012016>
- [40] Delgado-Friedrichs, O., O’Keeffe, M.: Identification of and symmetry computation for crystal nets. *Acta Crystallographica Section A* **59**(4), 351–360 (2003) <https://doi.org/10.1107/S0108767303012017>
- [41] Blöchl, P.E.: Projector augmented-wave method. *Physical Review B* **50**(24), 17953–17979 (1994) <https://doi.org/10.1103/PhysRevB.50.17953>
- [42] Perdew, J.P., Burke, K., Ernzerhof, M.: Generalized gradient approximation made simple. *Physical Review Letters* **77**(18), 3865–3868 (1996) <https://doi.org/10.1103/PhysRevLett.77.3865>
- [43] Kresse, G., Furthmüller, J.: Efficient iterative schemes for ab initio total-energy calculations using a plane-wave basis set. *Physical Review B* **54**(16), 11169–11186 (1996) <https://doi.org/10.1103/PhysRevB.54.11169>
- [44] Kresse, G., Joubert, D.: From Ultrasoft Pseudopotentials to the Projector Augmented-Wave Method Thermoelectric Properties of Transition Metal Oxides View project One dimensional Lattice Density Functional Theory View project From ultrasoft pseudopotentials to the projector augmen. *Physical Review B* **59**(3), 1758–1775 (1999) <https://doi.org/10.1103/PhysRevB.59.1758>

- [45] Bushlanov, P.V., Blatov, V.A., Oganov, A.R.: Topology-based crystal structure generator. *Computer Physics Communications* **236**, 1–7 (2019) <https://doi.org/10.1016/j.cpc.2018.09.016>
- [46] Jain, A., Ong, S.P., Hautier, G., Chen, W., Richards, W.D., Dacek, S., Cholia, S., Gunter, D., Skinner, D., Ceder, G., Persson, K.A.: Commentary: The materials project: A materials genome approach to accelerating materials innovation. *APL Materials* **1**(1), 11002 (2013) <https://doi.org/10.1063/1.4812323>
- [47] Sun, W., Dacek, S.T., Ong, S.P., Hautier, G., Jain, A., Richards, W.D., Gamst, A.C., Persson, K.A., Ceder, G.: The thermodynamic scale of inorganic crystalline metastability. *Science Advances* **2**(11), 1600225 (2016) <https://doi.org/10.1126/sciadv.1600225>

Supplementary Information:
Designing Superionic Conductors Using
Tetrahedrally Packed Structures

Tomoyasu Yokoyama^{1*}, Kazuhide Ichikawa¹, Takuya Naruse¹,
Kosei Ohura¹, Yukihiro Kaneko¹

^{1*}Technology Division, Panasonic Holdings Corporation, 1006 Kadoma,
Kadoma City, Osaka 571-8508, Japan.

*Corresponding author(s). E-mail(s):
yokoyama.tomoyasu@jp.panasonic.com;

Table S1: List of 45 Ag-ion conductors extracted from ICSD. “ICSD ID” refers to the Collection Code of the database. “Framework type” refers to the structural type of the anionic framework of each compound.

ICSD ID	Formula	Framework type
413508	Ag ₅ Te ₂ Cl	Al ₂ Cu
83282	Ag ₈ TiS ₆	MgCu ₂
54056	Ag ₇ PSe ₆	MgCu ₂
241154	Ag ₇ GeSe ₅ I	MgCu ₂
100267	Ag ₈ GeTe ₆	MgCu ₂
51487	Ag _{6.684} GeSe ₅ I _{0.69}	MgCu ₂
51488	Ag _{6.72} GeSe ₅ I _{0.69}	MgCu ₂
40957	Ag ₇ NbS ₆	MgCu ₂
29704	Cu _{1.5} Ag _{1.5} PS ₄	Li ₂ BaGe
29706	Ag ₃ PS ₄	Li ₂ BaGe
173113	Ag ₁₀ Te ₄ Br ₃	Zr ₄ Al ₃
159854	Ag ₃ SI _{0.4} Br _{0.6}	BCC
93448	AgHg _{0.5} I ₂	BCC
159851	Ag ₃ SI _{0.8} Br _{0.2}	BCC
159852	Ag ₃ SI _{0.67} Br _{0.33}	BCC
159857	Ag ₃ SI _{0.05} Br _{0.95}	BCC
159855	Ag ₃ SI _{0.25} Br _{0.75}	BCC
159856	Ag ₃ SI _{0.17} Br _{0.83}	BCC
159853	Ag ₃ SI _{0.6} Br _{0.4}	BCC
93429	Ag ₃ SI	BCC
2108	AgI	BCC
93428	Ag ₃ SI	BCC
200256	AgI	BCC
201003	Ag _{2.88} SI	BCC
9587	Ag ₂ S	BCC
9586	Ag ₂ S	BCC
93430	Ag ₃ SI	BCC
174096	Ag ₃ SBr	BCC
190397	Ag ₂ S	FCC
95608	Ag _{0.667} Pb _{0.167} I	FCC
95609	Ag _{0.5} Pb _{0.25} I	FCC
190590	Ag _{2.4} Sn _{0.8} I ₄	FCC
190587	Ag ₂ CdI ₄	FCC
190588	Ag ₂ ZnI ₄	HCP
190589	AgZn _{0.5} I ₂	HCP
93447	AgHg _{0.5} I ₂	HCP
601918	Ag _{0.144} Ga _{1.286} S ₂	HCP
51909	RbAg ₄ I ₅	β -Mn
41591	RbAg ₄ I ₅	β -Mn
33403	CsAg _{3.482} I _{2.999} Br _{1.998}	β -Mn

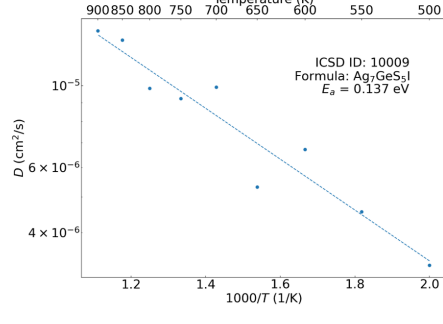
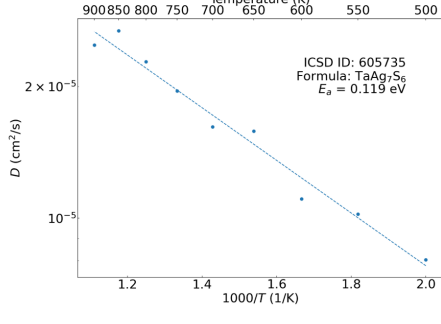
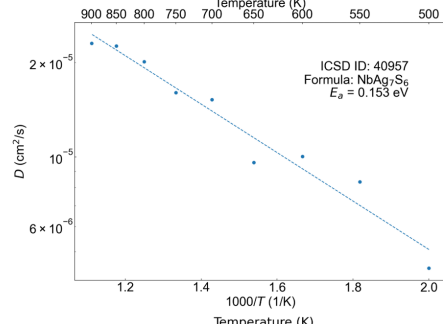
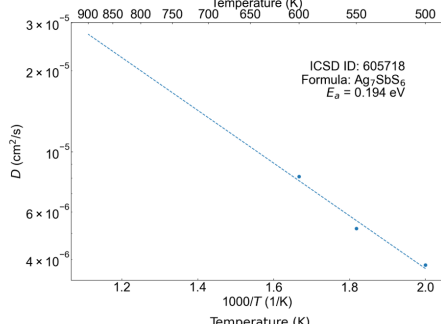
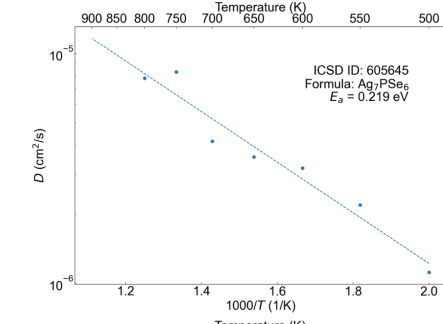
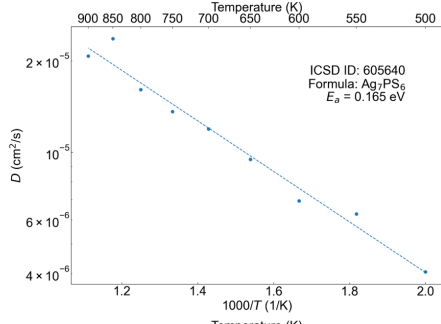
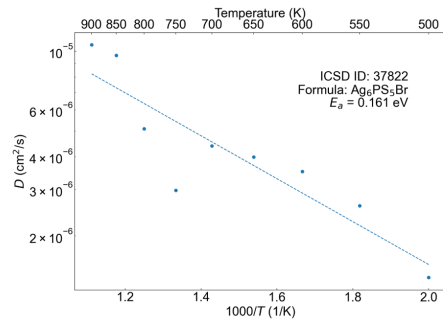
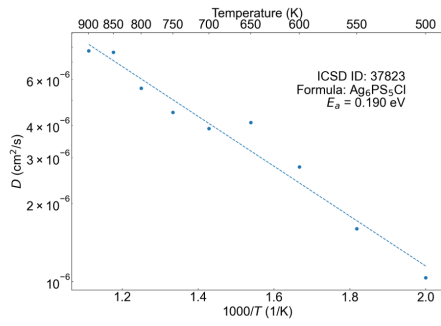
33401	CsAg _{3.668} I _{2.33} Br _{2.67}	β -Mn
33402	CsAg _{3.598} I _{2.669} Br _{2.331}	β -Mn
33400	CsAg _{3.446} I _{2.237} Br _{2.763}	β -Mn
27203	RbAg ₄ I ₅	β -Mn
51910	KAg _{3.925} I ₅	β -Mn

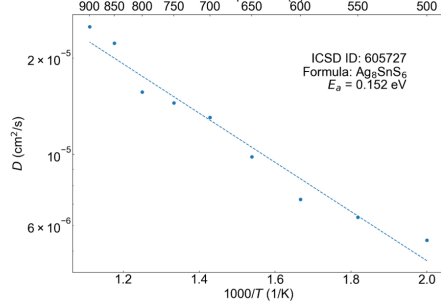
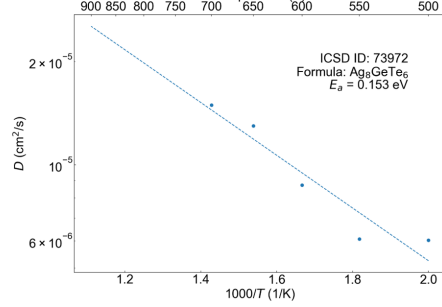
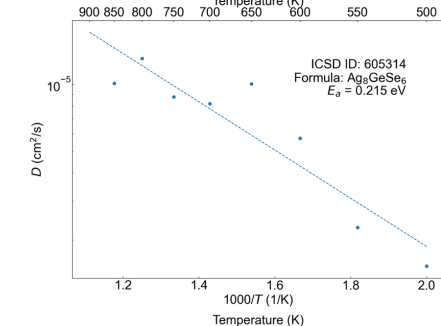
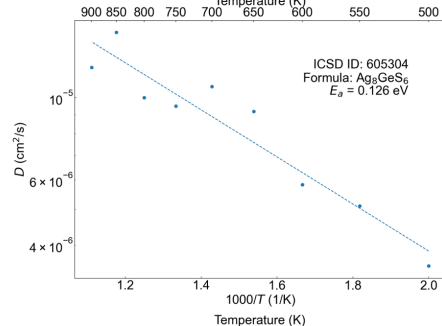
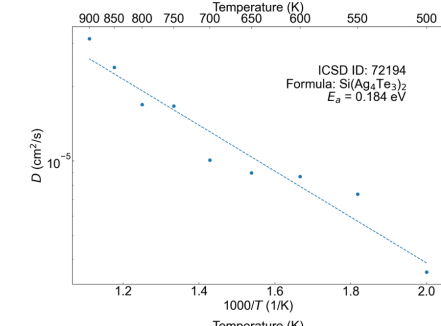
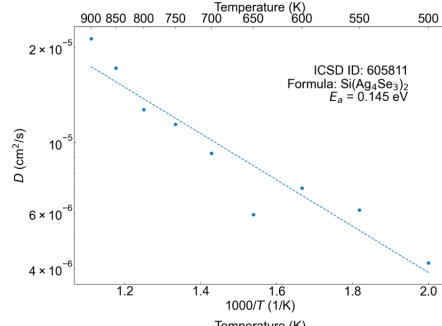
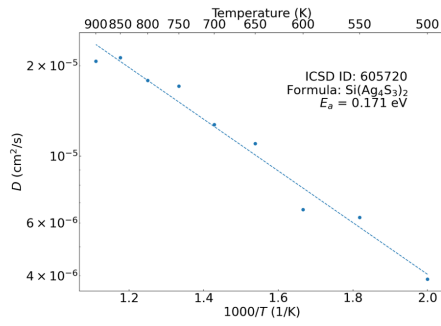
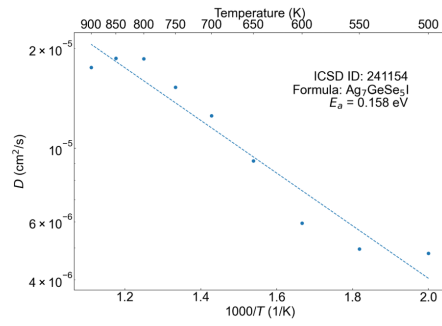
Table S2: List of the calculated ionic conductivities and activation energies of the Ag-, Cu-, Li-, Na-, Zn-, Cd-, Mg-, and F-ion TP framework compounds. “Ion” refers to a possible mobile ion in the compound. “Formula” refers to the compositional formula of the calculated structure. “ICSD ID” refers to the database collection code. “Framework type” refers to the structural type of the anion framework for each compound. σ_{300K} and $E_{a,300K}$ mean the ionic conductivity at room temperature and the activation energy as extrapolated from Arrhenius plots based on FPMD calculations, respectively. Estimates of the upper and lower limits of the ionic conductivity and the activation energy are included. If the ion conductivity is difficult to evaluate because the ions hardly diffuse, the ion conductivity and activation energy columns are labeled “Too Low” and “Too High”, respectively.

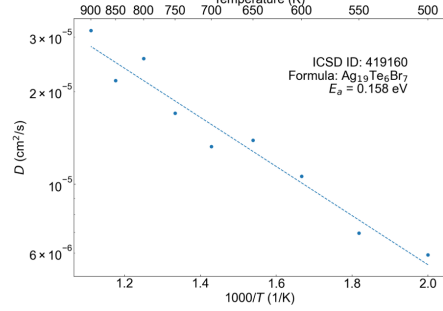
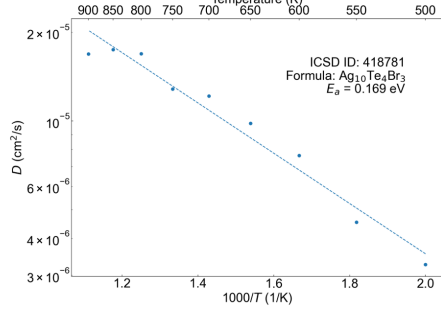
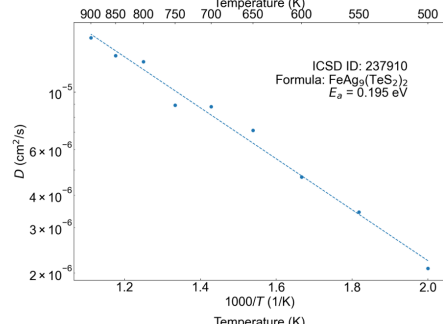
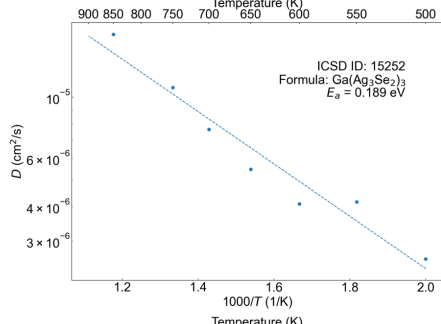
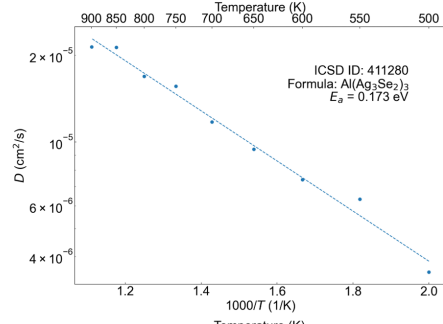
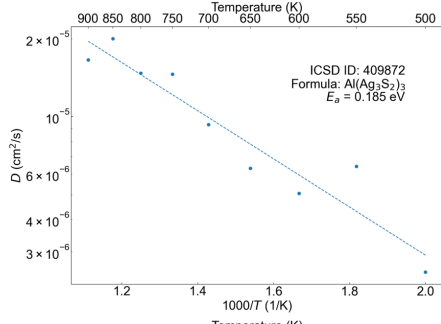
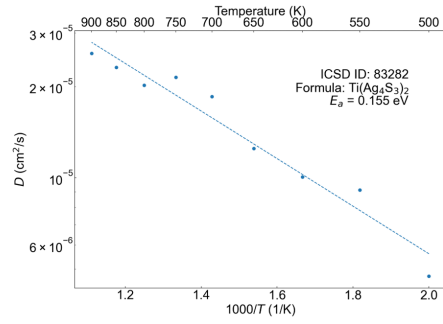
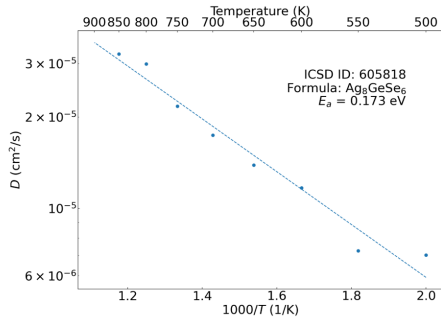
Ion	ICSD ID	Formula	Framework type	σ_{300K} (mS/cm)	$E_{a,300K}$ (eV)
Ag ⁺	37823	Ag ₆ PS ₅ Cl	MgCu ₂	8.1 (4.8, 13.8)	0.190±0.014
Ag ⁺	37822	Ag ₆ PS ₅ Br	MgCu ₂	16.3 (5.0, 53.2)	0.161±0.030
Ag ⁺	605640	Ag ₇ PS ₆	MgCu ₂	47.4 (32.4, 69.4)	0.165±0.010
Ag ⁺	605645	Ag ₇ PSe ₆	MgCu ₂	5.8 (2.4, 13.9)	0.219±0.023
Ag ⁺	605718	Ag ₇ SbS ₆	MgCu ₂	26.3 (8.4, 82.9)	0.194±0.030
Ag ⁺	40957	Ag ₇ NbS ₆	MgCu ₂	71.1 (43.9, 115.0)	0.153±0.012
Ag ⁺	605735	Ag ₇ TaS ₆	MgCu ₂	183.4 (138.0, 243.8)	0.119±0.007
Ag ⁺	10009	Ag ₇ GeS ₅ I	MgCu ₂	56.8 (31.8, 101.6)	0.137±0.015
Ag ⁺	241154	Ag ₇ GeSe ₅ I	MgCu ₂	46.3 (25.3, 84.8)	0.158±0.016
Ag ⁺	605720	Ag ₈ SiS ₆	MgCu ₂	47.6 (31.9, 71.1)	0.171±0.010
Ag ⁺	605811	Ag ₈ SiSe ₆	MgCu ₂	61.7 (30.6, 124.5)	0.145±0.018
Ag ⁺	72194	Ag ₈ SiTe ₆	MgCu ₂	29.0 (14.3, 58.8)	0.184±0.018
Ag ⁺	605304	Ag ₈ GeS ₆	MgCu ₂	89.0 (49.2, 161.1)	0.126±0.015
Ag ⁺	605314	Ag ₈ GeSe ₆	MgCu ₂	10.1 (2.4, 41.7)	0.215±0.037
Ag ⁺	73972	Ag ₈ GeTe ₆	MgCu ₂	63.5 (21.3, 189.1)	0.153±0.028
Ag ⁺	605727	Ag ₈ SnS ₆	MgCu ₂	68.5 (44.3, 105.9)	0.152±0.011
Ag ⁺	605818	Ag ₈ SnSe ₆	MgCu ₂	59.2 (35.5, 98.8)	0.173±0.013
Ag ⁺	83282	Ag ₈ TiS ₆	MgCu ₂	83.8 (50.6, 138.8)	0.155±0.013
Ag ⁺	409872	Ag ₉ AlS ₆	MgCu ₂	30.1 (12.6, 72.0)	0.185±0.023
Ag ⁺	411280	Ag ₉ AlSe ₆	MgCu ₂	43.4 (32.3, 58.3)	0.173±0.008
Ag ⁺	15252	Ag ₉ GaSe ₆	MgCu ₂	20.6 (9.4, 45.2)	0.189±0.020
Ag ⁺	237910	Ag ₉ FeTe ₂ S ₄	MgCu ₂	18.0 (13.1, 24.9)	0.195±0.008
Ag ⁺	418781	Ag ₁₀ Te ₄ Br ₃	Zr ₄ Al ₃	38.2 (24.0, 61.0)	0.169±0.012
Ag ⁺	419160	Ag ₁₉ Te ₆ Br ₇	W ₆ Fe ₇	71.6 (43.1, 118.9)	0.158±0.013
Ag ⁺	51910	KAg ₄ I ₅	β -Mn	18.6 (10.4, 33.1)	0.172±0.015
Ag ⁺	27203	RbAg ₄ I ₅	β -Mn	48.3 (26.5, 88.0)	0.139±0.016
Ag ⁺	421400	Ag ₅ Te ₂ Cl	Al ₂ Cu	14.8 (7.7, 28.1)	0.206±0.017
Ag ⁺	18540	K ₂ Ag ₂ SnS ₄	CrB	Too low	Too high
Ag ⁺	80195	Cs ₂ Ag ₂ ZrTe ₄	CrB	Too low	Too high
Ag ⁺	55840	CsAgZnS ₂	CrB	Too low	Too high
Cu ⁺	418657	Cu ₆ PS ₅ Cl	MgCu ₂	1.0 (0.3, 2.9)	0.275±0.028
Cu ⁺	33503	Cu ₆ PS ₅ Br	MgCu ₂	Too low	Too high

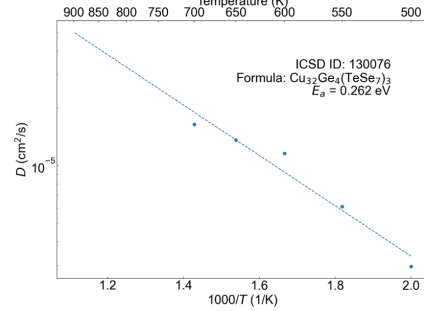
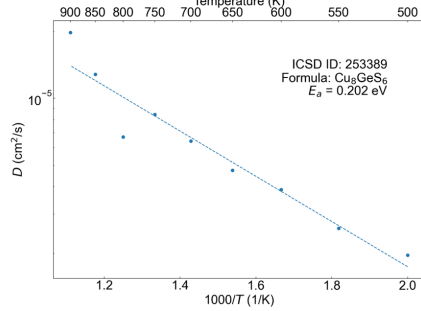
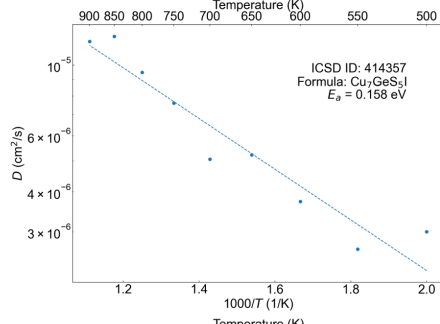
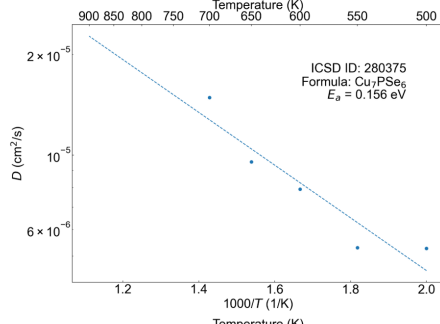
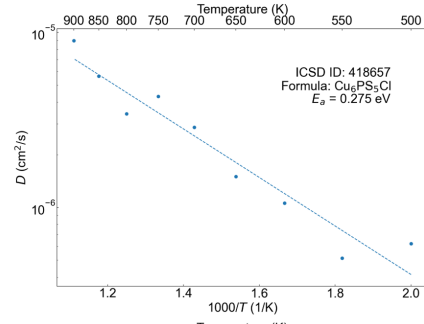
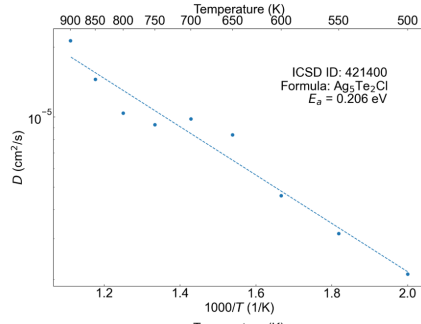
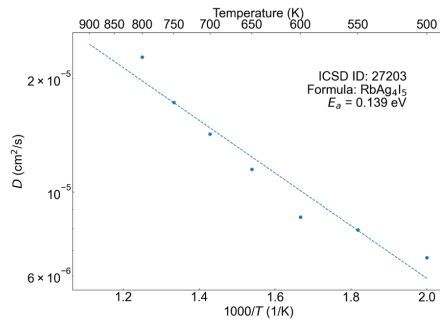
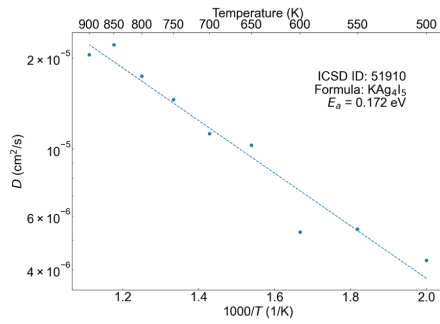
Cu ⁺	415489	Cu ₆ P ₁ S ₅ I	MgCu ₂	Too low	Too high
Cu ⁺	280375	Cu ₇ PSe ₆	MgCu ₂	67.6 (19.3, 236.5)	0.156±0.032
Cu ⁺	414357	Cu ₇ GeS ₅ I	MgCu ₂	33.9 (16.9, 67.7)	0.158±0.018
Cu ⁺	253389	Cu ₈ GeS ₆	MgCu ₂	15.2 (6.6, 35.0)	0.202±0.022
Cu ⁺	253394	Cu ₈ GeSe ₆	MgCu ₂	Too low	Too high
Cu ⁺	130076	Cu ₈ GeTe ₂ Se ₄	MgCu ₂	9.9 (2.7, 35.9)	0.262±0.033
Cu ⁺	88660	Cu ₈ GeSe ₆	MgZn ₂	0.5 (0.1, 3.0)	0.403±0.048
Cu ⁺	610355	Cu ₆ SbAs	Cr ₃ Si	0.8 (0.2, 3.2)	0.233±0.037
Cu ⁺	427561	Cu ₆ Te ₃ S	Cr ₃ Si	8.5 (4.6, 16.0)	0.246±0.016
Cu ⁺	140304	Cu ₉ Te ₄ Cl ₃	Zr ₄ Al ₃	40.9 (20.1, 83.1)	0.177±0.018
Cu ⁺	51911	KCu ₄ I ₅	β-Mn	31.9 (19.6, 51.8)	0.164±0.013
Cu ⁺	201347	Cu ₃ B ₇ O ₁₃ Br	NaZn ₁₃	Too low	Too high
Cu ⁺	61058	Cu ₃ B ₇ O ₁₃ I	NaZn ₁₃	Too low	Too high
Li ⁺	421479	Li ₆ PO ₅ Cl	MgCu ₂	Too low	Too high
Li ⁺	421480	Li ₆ PO ₅ Br	MgCu ₂	Too low	Too high
Li ⁺	418490	Li ₆ PS ₅ Cl	MgCu ₂	10.6 (4.7, 23.9)	0.180±0.021
Li ⁺	122370	Li ₆ PS ₅ Br	MgCu ₂	6.6 (3.6, 11.9)	0.174±0.015
Li ⁺	380388	Li ₆ AsS ₅ Br	MgCu ₂	5.7 (2.9, 11.2)	0.210±0.017
Li ⁺	418489	Li ₆ PS ₅ I	MgCu ₂	7.1 (3.9, 12.9)	0.151±0.015
Li ⁺	144313	Li ₆ PSe ₅ I	MgCu ₂	4.7 (2.9, 7.8)	0.184±0.013
Li ⁺	380389	Li ₆ AsS ₅ I	MgCu ₂	5.5 (2.7, 11.5)	0.161±0.019
Li ⁺	421130	Li ₇ PS ₆	MgCu ₂	2.5 (1.1, 5.9)	0.299±0.022
Li ⁺	421131	Li ₇ PSe ₆	MgCu ₂	79.6 (49.8, 127.0)	0.183±0.012
Li ⁺	85713	Li ₇ N ₂ I	MgCu ₂	1.1 (0.4, 3.7)	0.281±0.030
Li ⁺	247255	Li ₈ N ₂ Se	MgCu ₂	Too low	Too high
Li ⁺	247258	Li ₈ N ₂ Te	MgCu ₂	Too low	Too high
Li ⁺	143283	Li ₆ SiO ₄ Cl ₂	MgZn ₂	0.3 (0.1, 1.0)	0.199±0.027
Li ⁺	167528	Li ₃ (NH ₂) ₂ I	MgZn ₂	5.3 (2.5, 11.3)	0.217±0.019
Li ⁺	402881	LiGa ₃ Te ₅	β-Mn	Too low	Too high
Li ⁺	55064	Li(NH ₃)I	CrB	Too low	Too high
Li ⁺	74930	Li ₂ (OH)I	FeB	Too low	Too high
Li ⁺	143928	Li ₆ B ₇ S ₁₃ I	NaZn ₁₃	2.1 (1.1, 4.1)	0.247±0.017
Na ⁺	253640	Na ₂ CdGe ₂ Se ₆	MgZn ₂	Too low	Too high
Na ⁺	402329	NaGa ₃ Te ₅	β-Mn	Too low	Too high
Na ⁺	243562	NaIn ₂ GaSe ₅	β-Mn	Too low	Too high
Na ⁺	402879	NaGa ₆ AgTe ₁₀	β-Mn	Too low	Too high
Na ⁺	12964	CsNaMnTe ₂	CrB	Too low	Too high
Na ⁺	47100	NaGe ₂ N ₃	CaCu ₅	Too low	Too high
Zn ²⁺	420783	ZnHg ₃ S ₂ Cl ₄	MgZn ₂	Too low	Too high
Zn ²⁺	65257	Cs ₂ Mn ₂ ZnS ₄	CrB	Too low	Too high
Zn ²⁺	55444	Zn ₃ B ₇ O ₁₃ Cl	NaZn ₁₃	Too low	Too high
Cd ²⁺	622	Cd ₁₃ P ₄ S ₂₂ I ₂	MgCu ₂	0.7 (0.1, 2.9)	0.279±0.039
Cd ²⁺	84983	Cd ₈ As ₇ Cl	Cr ₃ Si	Too low	Too high
Cd ²⁺	85581	CsCdAuS ₂	CrB	Too low	Too high
Mg ²⁺	22009	Mg ₃ B ₇ O ₁₃ Cl	NaZn ₁₃	Too low	Too high

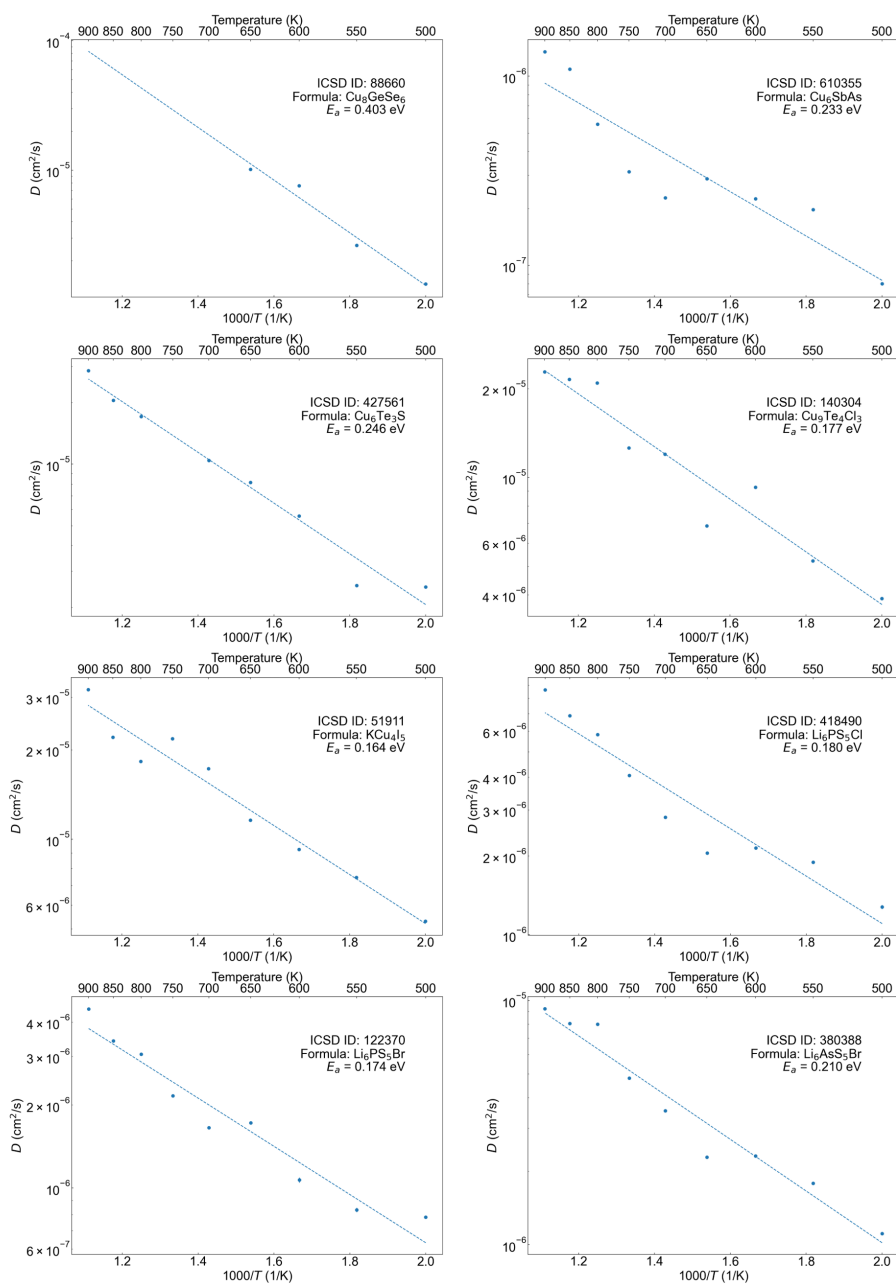
F ⁻	14136	NaSn ₂ F ₅	Al ₂ Cu	1.8 (0.2, 14.9)	0.432±0.055
F ⁻	431489	KSbF ₄	FeB	1.5 (0.3, 8.1)	0.332±0.043

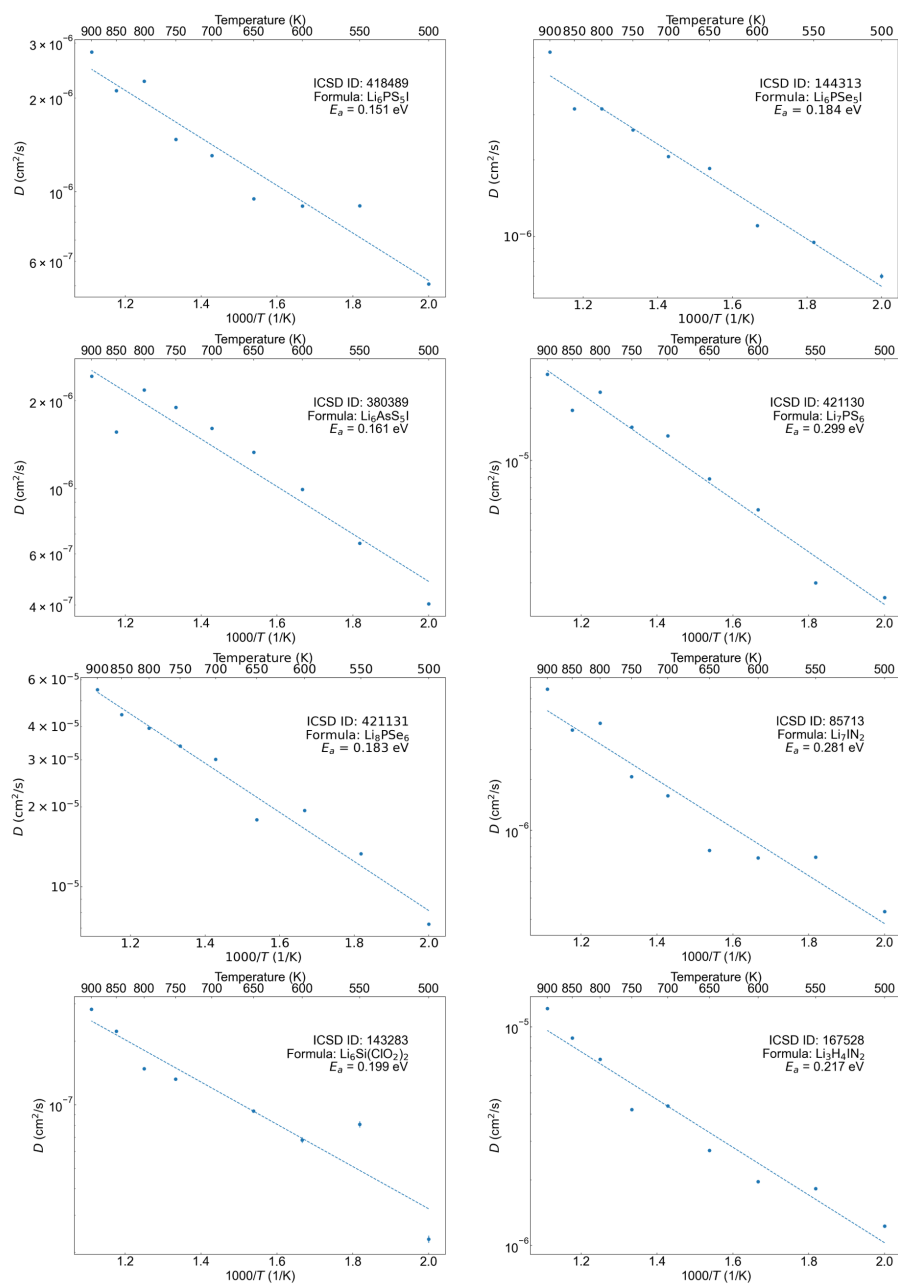












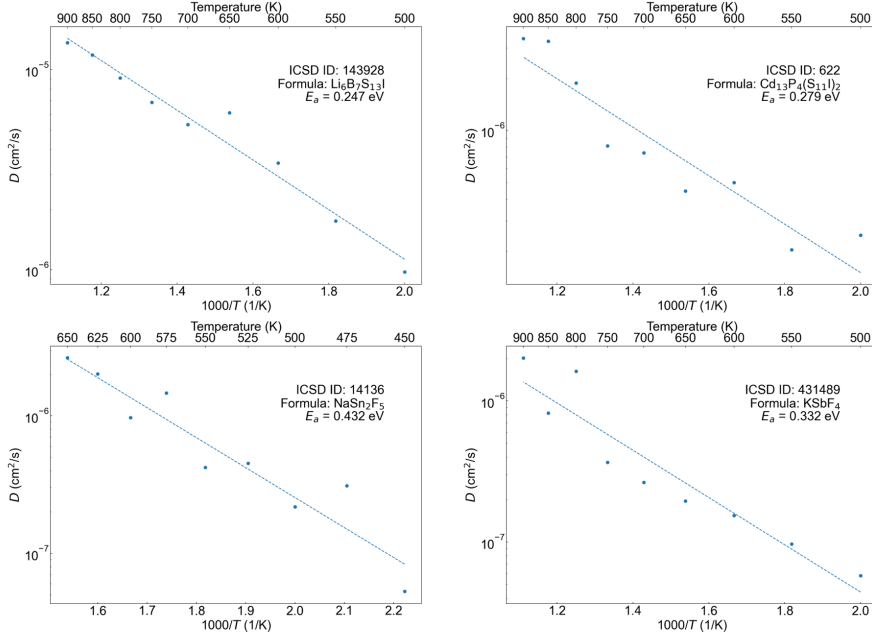


Fig. S1 Arrhenius plots for TP framework compounds in the ICSD obtained by first-principles molecular dynamics calculations.

Table S3: List of Li-ion conductor candidates screened using the Me2Ion method under the conditions that $E_{hull} < 0.1$ eV/atom and $\sigma_{300K} > 1 \times 10^{-3}$ S/cm. “Ion” refers to a possible mobile ion in the compound. “Formula” refers to the compositional formula of the calculated structure. “Framework type” refers to the structural type of the anionic framework for each compound. E_{hull} represents the convex hull energy, which is an index of the thermodynamic stability obtained from first-principles calculations. σ_{300K} and $E_{a,300K}$ mean the ionic conductivity at room temperature and the activation energy as extrapolated from Arrhenius plots based on FPMD calculations, respectively.

Ion	Formula	Framework type	E_{hull} (eV/atom)	σ_{300K} (S/cm)	$E_{a,300K}$ (eV)
Li ⁺	Li ₄ InAs ₂ F	Al ₂ Cu	0.099	8.0×10^{-2}	0.171
Li ⁺	Li ₄ InP ₂ F	Al ₂ Cu	0.095	3.6×10^{-2}	0.204
Li ⁺	Li ₄ InSb ₂ Cl	Al ₂ Cu	0.091	3.1×10^{-2}	0.192
Li ⁺	Li ₃ SiP ₂ Cl	Al ₂ Cu	0.093	1.2×10^{-2}	0.242
Li ⁺	Li ₄ InAs ₂ Cl	Al ₂ Cu	0.077	2.0×10^{-3}	0.294
Li ⁺	Li ₄ AlAs ₂ F	Al ₂ Cu	0.072	1.6×10^{-3}	0.330

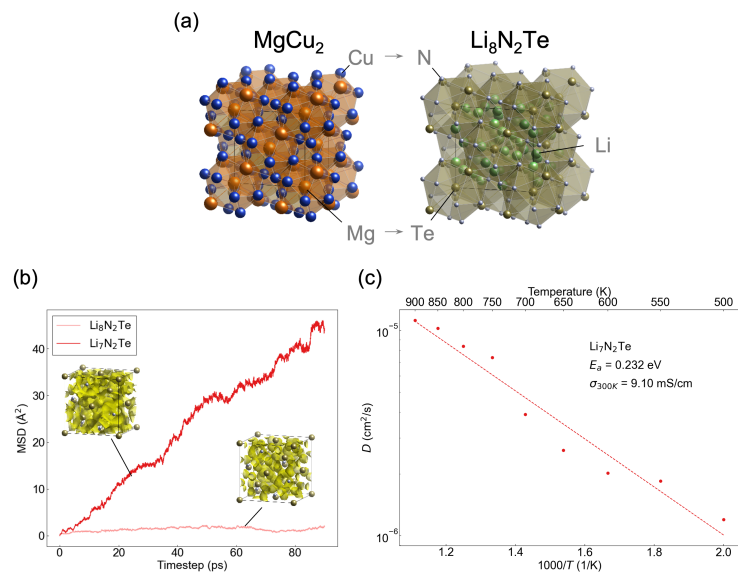


Fig. S2 (a) Crystal structures of MgCu_2 and $\text{Li}_8\text{N}_2\text{Te}$ with MgCu_2 -type framework. (b) Li-ion diffusion paths and mean square displacement (MSD) of Li ions of $\text{Li}_8\text{N}_2\text{Te}$ and $\text{Li}_7\text{N}_2\text{Te}$, and (c) Arrhenius plots of $\text{Li}_7\text{N}_2\text{Te}$ obtained by first-principles molecular dynamics calculations.

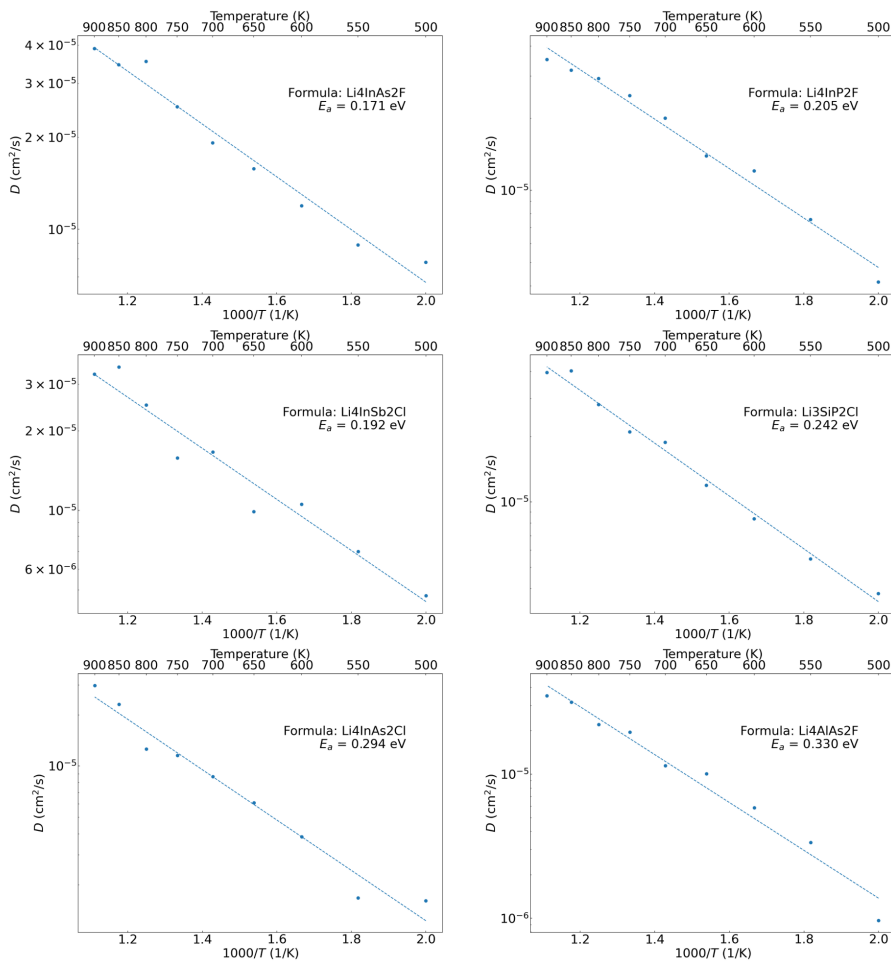


Fig. S3 Arrhenius plots for Li-ion conductor candidates with Al_2Cu -type framework listed in Table S3 obtained by first-principles molecular dynamics calculations.